

Article

An Enhanced Power Allocation Strategy for Microgrids Considering Frequency and Voltage Restoration

Chunguang Yang ¹, Xue Wu ², Qichao Song ^{1,*}, Haoyu Wu ² and Yixin Zhu ²¹ School of Control Technology, Wuxi Institute of Technology, Wuxi 214121, China; yangcg@wxit.edu.cn² School of Lot Engineering, Jiangnan University, Wuxi 214122, China; 6231915004@stu.jiangnan.edu.cn (X.W.); 6211925024@stu.jiangnan.edu.cn (H.W.); yixinzhu1987@jiangnan.edu.cn (Y.Z.)

* Correspondence: songqc@wxit.edu.cn

Abstract: In a microgrid, load power should be properly shared among multiple distributed generation (DG) units, not only for fundamental power but also for negative sequence and harmonic power. In this paper, the operation of a microgrid under imbalance and nonlinear load conditions is studied, and a consensus algorithm-based distributed control strategy is proposed for the microgrid power allocation, frequency, and voltage restoration. First of all, the output current of DG unit is decomposed by second-order generalized integrator (SOGI) modules to obtain the fundamental power and harmonic power through the power calculation formula. Then, state values of DG units, such as local power, frequency, and voltage, are transmitted on a sparse communication network. Under the action of a consensus algorithm, the real power of DG units is allocated following the equal increment principle; the reactive power, imbalance, and harmonic power are allocated according to the capacities of DG units; and the frequency of the microgrid and the voltage at the point of common coupling (PCC) are rated. In the consensus-based strategy, DG units only communicate with their neighbor units; thus, the “plug and play” function is reserved. Compared with the centralized control strategy, the proposed strategy with a distributed consensus protocol can simplify the maintenance and possible expansions of the system, making the microgrid more flexible. Moreover, as the structure of the detailed network is not required, it is easy to apply in practice. Simulation and experiment results are presented to verify the proposed method.

Keywords: microgrid; consensus algorithm; harmonic power; power allocation; frequency restoration

Citation: Yang, C.; Wu, X.; Song, Q.; Wu, H.; Zhu, Y. An Enhanced Power Allocation Strategy for Microgrids Considering Frequency and Voltage Restoration. *Electronics* **2024**, *13*, 1966. <https://doi.org/10.3390/electronics13101966>

Academic Editors: Antonio J. Marques Cardoso and Ahmed Abu-Siada

Received: 25 April 2024

Revised: 14 May 2024

Accepted: 15 May 2024

Published: 17 May 2024



Copyright: © 2024 by the authors. Licensee MDPI, Basel, Switzerland. This article is an open access article distributed under the terms and conditions of the Creative Commons Attribution (CC BY) license (<https://creativecommons.org/licenses/by/4.0/>).

1. Introduction

A microgrid is an effective way to increase the penetration of distributed generation (DG) into the main grid [1]. It is capable of operating either in grid-connected or in islanded mode, thereby increasing the supply reliability for the end user. A microgrid provides a promising solution to integrate multiple renewable energy resources and storage systems. At present, research on microgrids is mainly on the subject of architecture, modeling, stability analysis, power quality improvement, and power sharing, etc.

In an islanded microgrid, load demand should be properly shared among multiple DG units. That means each DG unit should output power in proportion to its power rating if there is no management of the microgrid central controller (MGCC) or consideration of economic benefits. Normally, the frequency and voltage amplitude droop control method can be used to improve the distributed mode to achieve microgrid power sharing [2,3]. Due to its wireless control characteristic, the “plug and play” function of DG units is enabled. While frequency droop control allows for precise actual power sharing due to frequency uniformity, voltage droop control often results in poor reactive power sharing due to mismatched feeder impedances and different offsets of local loads [4].

In recent years, various modified droop control methods have been developed to deal with the reactive power sharing issue. In [5,6], predominant virtual inductors were placed

at DG unit outputs, which mainly aimed to prevent the power control instability. In [7], a comprehensive treatment about virtual impedance concept is presented. Emphasis is placed on mismatched feeders connected to the point of common coupling (PCC) and the effects of local loads are ignored. In [8], both the DG unit feeder and local load are considered. Due to the introduced feeder current sensing, dynamic power sharing among DG units is achieved. However, when the microgrid structure is networked, the above wireless methods cannot provide a satisfactory reactive power sharing effect.

To solve the reactive power sharing issue in networked microgrids, communication-based solutions become shortcuts. In [9,10], a synchronizing signal is utilized to trigger an extra regulation process for reactive power sharing, but the control performance is easy to influence if the load changes during the regulation period. With the communication links between MGCC and DG units, reactive power sharing can be easily achieved through secondary regulation [11–13]. In recent years, a distributed control method based on a multi-agent consensus protocol has also been developed, which only uses a sparse communication network (SCN) [14–18]. Different from the MGCC-based centralized control strategy, DG units in SCN only communicate with their neighbor units.

On the other hand, the microgrid may have serious power quality issues due to intensive imbalance and nonlinear loads. Similar to the situation of reactive power sharing, mismatched feeder impedance in a weak microgrid can also cause imbalance and harmonic power sharing issues. Thus, virtual impedances at fundamental negative sequence and selected harmonic frequencies are developed to achieve imbalance and harmonic power sharing [19,20]. However, as the MGCC is required, the reliability of the system may be reduced. In [21,22], consensus protocol-based control strategies are proposed to reduce the harmonic distortion of the DG unit voltage. Then, imbalance and harmonic power sharing issues are discussed in [23], and the corresponding consensus protocol is established based on imbalance and total harmonic power. But using the total harmonic power can hardly keep the harmonic power at each order well shared. In the above consensus-based control strategies, economic issues are not considered. In fact, as the SCN is introduced, power sharing should not be the only power allocation principle; economic factors and other performance indexes should also be considered [24–27].

This paper employs a consensus protocol to artificially deal with the various issues in microgrids. In the proposed strategy, there are three main distributed regulators: the Q-V regulator for reactive power sharing and voltage restoration; the P-f regulator for real power allocation and frequency restoration; and the I-H regulator for imbalance and harmonic power sharing. To realize more accurate harmonic power sharing, the harmonic power at each order is utilized. To realize economic optimization, the equal increment principle (EIP) is introduced. To realize smoother mode switching of the microgrid, the PCC voltage and microgrid frequency are regulated to the rated values. In this paper, microgrid control issues and the proposed consensus-based control strategy are introduced in Sections 2 and 3. Some simulation and experiment results are given to validate the proposed control strategy in Sections 4 and 5.

2. Microgrid and Issues

2.1. Droop Control in Microgrids

Figure 1 illustrates the structure of a networked microgrid. In such a microgrid, DG units can be connected to any node of the network. Some loads connected directly to DG units are called local loads, and the others are public loads. Like a traditional microgrid, by controlling the static transfer switch (STS) at the PCC, the networked microgrid can operate in either islanded or grid-connected mode. In grid-connected mode, as the voltage of microgrid is supported by the main grid, the power allocation issue can be easily solved by adopting power tracking techniques. However, in islanded mode, power sharing relies on the cooperation of multiple DG units.

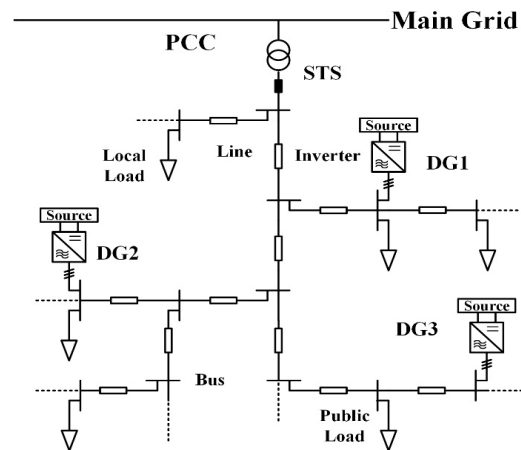


Figure 1. Illustration of a networked microgrid.

Normally, for islanded operation, DG units can employ the conventional frequency and voltage magnitude droop control as

$$\omega_i = \omega_{0i} - m_i P_i \quad (1)$$

$$E_i = E_{0i} - n_i Q_i \quad (2)$$

where ω_{0i} and E_{0i} are the initial values of the DG angle frequency and voltage magnitude, respectively; P_i and Q_i are the measured real and reactive power of the DG unit i ; and m_i and n_i are the real and reactive power droop slopes. Normally, they can be defined as

$$m_i = \frac{\omega_{max} - \omega_{min}}{P_i^*} \quad (3)$$

$$n_i = \frac{E_{max} - E_{min}}{Q_i^*} \quad (4)$$

where ω_{max} and ω_{min} are the upper and lower bounds of the microgrid frequency, respectively; E_{max} and E_{min} are the upper and lower bounds of the microgrid voltage, respectively; and P_i^* and Q_i^* are the rated real and reactive powers of the DG unit i , respectively. With the derived angle frequency and voltage magnitude, the instantaneous voltage reference of the DG unit can be obtained accordingly.

It can be seen from (3) and (4) that larger-capacity DG units will be set with smaller droop slopes. Thus, when all the DG units operate under the same frequency and voltage magnitude, larger-capacity DG units could output more real and reactive power according to (1) and (2). In practical application, due to the consistent frequency among DG units, the frequency droop control always achieves accurate real power sharing. However, as the voltage magnitudes of DG units are rarely unified due to the mismatched network input impedances, the voltage magnitude droop control typically suffers the reactive power sharing issue. In addition to this, the droop control also has some other issues:

- (1) When imbalance and nonlinear loads are connected to the microgrid, imbalance and harmonic power will be generated, which also need to be properly shared.
- (2) Real power sharing is a kind of power allocation strategy without considering economic factors of DG units. It mainly considers the operation of inverters.
- (3) Droop control has static errors in the frequency and voltage magnitude control. The influence is small in islanded mode, but large in the mode-switching process.

The droop control still needs to be improved.

2.2. Power Sharing Analysis

To analyze the relationship between DG output power and virtual impedance, a parallel system with two identical droop-controlled DG units is introduced, with its equivalent

circuit illustrated in Figure 2. As the figure shows, each DG unit is equivalent to a droop-controlled voltage source in series with its virtual impedance. Assuming that the DG units only output the fundamental positive sequence voltage, the equivalent circuit can be decomposed into the three circuits shown in Figure 2: the circuits at the fundamental positive sequence, at the fundamental negative sequence, and at the selected harmonic frequency.

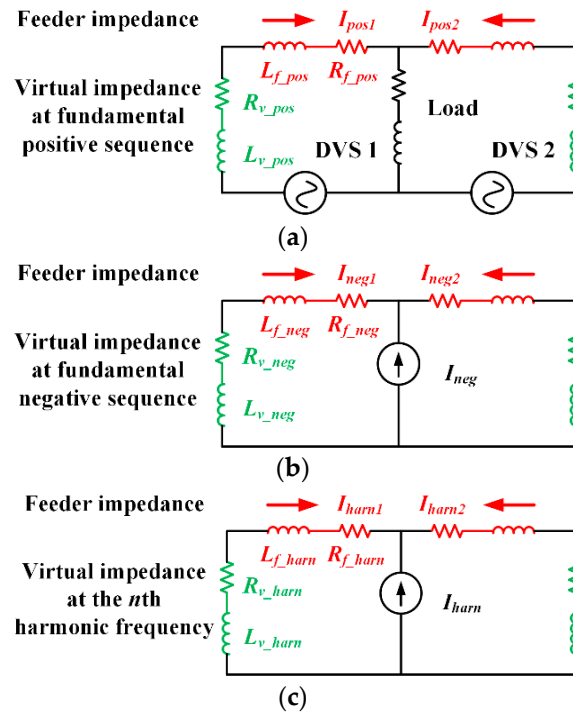


Figure 2. Equivalent circuits of a parallel system at different frequencies and sequences. (a) Equivalent circuit at the fundamental positive sequence. (b) Equivalent circuit at the fundamental negative sequence. (c) Equivalent circuit at selected harmonic frequency.

In Figure 2a, the PCC load is lumped as a passive RL load. In order to realize accurate real and reactive power sharing, DG units should have droop control slopes designed according to (3) and (4). Meanwhile, the impedances between DG units and the PCC should be equal.

$$L_{e_pos} = L_{f_pos} + L_{v_pos} \tag{5}$$

$$R_{e_pos} = R_{f_pos} + R_{v_pos} \tag{6}$$

where L_{e_pos} and R_{e_pos} are the equivalent inductance and resistance at the fundamental positive sequence, respectively; L_{f_pos} and R_{f_pos} are the physical inductance and resistance at the fundamental positive sequence, respectively; and L_{v_pos} and R_{v_pos} are the virtual inductance and resistance at the fundamental positive sequence, respectively. By regulating L_{v_pos} and R_{v_pos} , making sure each DG unit has the same L_{e_pos} and R_{e_pos} , DG units will output the same reactive power.

The equivalent circuit at the fundamental negative sequence is presented in Figure 2b, where the imbalanced load at PCC is described as a current source I_{neg} . In this system, the equivalent impedance at the fundamental negative sequence is

$$L_{e_neg} = L_{f_neg} + L_{v_neg} \tag{7}$$

$$R_{e_neg} = R_{f_neg} + R_{v_neg} \tag{8}$$

where L_{e_neg} and R_{e_neg} are the equivalent inductance and resistance at the fundamental negative sequence, respectively; L_{f_neg} and R_{f_neg} are the physical inductance and resistance at the fundamental negative sequence, respectively; and L_{v_neg} and R_{v_neg} are the virtual

inductance and resistance at the fundamental negative sequence, respectively. If each DG unit has the same L_{e_neg} and R_{e_neg} , the DG units will output the same imbalance power. The equivalent circuit at the selected harmonic frequency is presented in Figure 2c. The equivalent impedance at the n th harmonic frequency is

$$L_{e_han} = L_{f_han} + L_{v_han} \quad (9)$$

$$R_{e_han} = R_{f_han} + R_{v_han} \quad (10)$$

where L_{e_han} and R_{e_han} are the equivalent inductance and resistance at the n th harmonic frequency, respectively; L_{f_han} and R_{f_han} are the physical inductance and resistance at the n th harmonic frequency, respectively; L_{v_han} and R_{v_han} are the virtual inductance and resistance at the n th harmonic frequency, respectively. Similarly, the L_{e_han} and R_{e_han} of each DG unit should remain equal.

Based on the assumption of main inductive DG equivalent impedance and slow microgrid load demand dynamics, the relationship between DG output power and virtual impedance can be summarized as

$$\begin{cases} Z_{v_pos} \uparrow \Rightarrow Q_{pos} \downarrow \\ Z_{v_neg} \uparrow \Rightarrow Q_{neg} \downarrow \\ Z_{v_han} \uparrow \Rightarrow Q_{han} \downarrow \end{cases} \quad (11)$$

where Q_{pos} , Q_{neg} , and Q_{han} are the DG reactive, imbalance, and n th harmonic power, respectively. The detailed definition will be given in the next section. It can be seen that by increasing the virtual impedance value, the related power component of the DG unit can be reduced, and vice versa.

2.3. Preliminaries on Consensus Algorithm

Before introducing the proposed strategy, some preliminary knowledge of graph theory should be briefly presented first. For distributed control of DG units, directed graph (digraph) can be used to describe the microgrid topology. A digraph is usually expressed as $G = (V_G, E_G, A_G)$, which consists of a node set $V_G = \{v_1, v_2, \dots, v_n\}$, an edge set $E_G \subseteq V_G \times V_G$, and the associated adjacency matrix $A_G = [a_{ij}]$. The nodes of the digraph denote each DG agent in a microgrid, and the edges denote communication links between DG units. Each edge $(v_i, v_j) \in E_G$ represents that agent i obtains information from agent j . The set of neighbors of the i th vertex is denoted as $N_i = \{j \mid (v_i, v_j) \in E_G\}$. The elements of the adjacency matrix A_G are defined as $a_{ij} = a_{ji} = 1$ if $j \in N_i$; otherwise, $a_{ij} = a_{ji} = 0$. For a digraph, if node j is the neighbor of node i , then node i can obtain information from node j , but not necessarily vice versa. The in-degree matrix is defined as $D = \text{diag}\{d_i\}$ with $d_i = \sum_{j \in N_i} a_{ij}$. The Laplacian matrix L is defined as $L = D - A_G$. In the leader adjacency matrix $F = [f_j]_{N \times 1}$, if the i th node can receive information from the reference value, it is called the pinning node with $f_i = 1$, otherwise $f_j = 0$. When there exists at least a direct path from the root node to every other node in the digraph, the digraph is said to have a spanning tree.

Taking the sparse information into account, the proposed consensus-based control strategy is modelled by a digraph based on the above graph theory. The scalar information state x_i is bound to each communication node i . Node i will update its information with its own information and that of its neighbor. By reaching a consensus, it means each node asymptotically converges to the same state. According to the related literature [28,29], the update rule is based on the solution of continuous consensus algorithms for the regulator synchronization problem and tracking synchronization problem, respectively.

In [28], it is pointed out that if each node i in the digraph can receive information from its neighbors, then all the nodes of the digraph globally, asymptotically reach an average consensus. Meanwhile, in [29], it is pointed out that if the information of leader node i can be used in a local controller, all nodes in the digraph can follow the set value of the leader node even its value changes over time.

As described above, the update rule can be summarized as

$$\dot{x}_i(t) = - \sum_{j \in N_i} a_{ij} [x_i(t) - x_j(t)] \tag{12}$$

$$\dot{x}_i(t) = - \sum_{j \in N_i} a_{ij} [x_i(t) - x_j(t)] - g_i [x_i(t) - x_{ref}] \tag{13}$$

where the pinning gain $g_i \geq 0$ if node i is the leader of the digraph which is connected to the reference. It is non-zero only for a few root nodes (at least one root node) with the reference value x_{ref} . If the communication network contains a spanning tree, the rules above can be achieved. Then, in the regulator synchronization problem, the states of the nodes synchronize to a common value that is not prescribed, and in the tracking synchronization problem, the node states synchronize to the reference value x_{ref} . For the proposed control, the power allocation issue corresponds to the regulator synchronization problem, and the voltage and frequency restoration issue corresponds to the tracking synchronization problem.

3. Consensus-Based Control Strategy

As previously mentioned, the proposed control strategy contains three regulators: the Q-V regulator, P-f regulator, and I-H regulator.

3.1. I-H Regulator for Imbalance and Harmonic Power Sharing

3.1.1. Imbalance and Harmonic Power Detection

By using the second-order generalized integrator (SOGI) method in [27], the fundamental and harmonic currents can be separated. The simplified decomposition diagram is sketched in Figure 3.

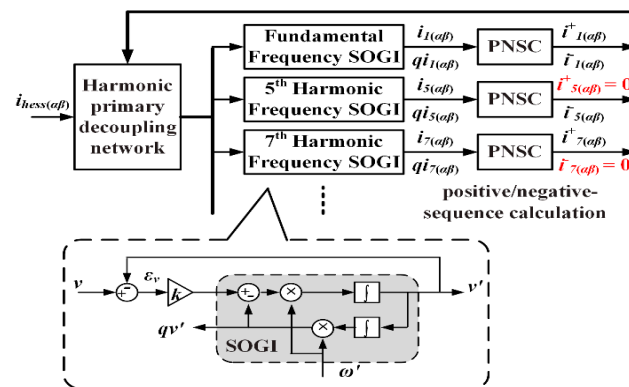


Figure 3. Decomposition of the fundamental positive sequence, fundamental negative sequence, and harmonic currents.

Firstly, the three-phase currents are transferred into the α and β two phases. Then, through the filtering function of the SOGI block, the specific harmonic currents are extracted. Finally, the detected currents are sent to the positive/negative sequence calculation (PNSC) block to further separate the positive and negative sequence components. The transformations in the PNSC are as follows:

$$v_{\alpha\beta}^+ = \frac{1}{2} \begin{bmatrix} 1 & -q \\ q & 1 \end{bmatrix} v_{\alpha\beta} \tag{14}$$

$$v_{\alpha\beta}^- = \frac{1}{2} \begin{bmatrix} 1 & q \\ -q & 1 \end{bmatrix} v_{\alpha\beta} \tag{15}$$

where

$$v_{\alpha\beta} = \sqrt{\frac{2}{3}} \begin{bmatrix} 1 & -\frac{1}{2} & -\frac{1}{2} \\ 0 & \frac{\sqrt{3}}{2} & -\frac{\sqrt{3}}{2} \end{bmatrix} v_{abc}$$

$$q = e^{-j(\pi/2)}$$

and q is a 90° -lagging, phase-shifting operator applied to the time domain to obtain an in-quadrature version of the input waveforms. With the detected current components, the fundamental positive/negative and harmonic powers can be calculated as

$$P = V_\alpha I_{1\alpha}^+ + V_\beta I_{1\beta}^+ \quad (16)$$

$$Q = V_\beta I_{1\alpha}^+ - V_\alpha I_{1\beta}^+ \quad (17)$$

$$Q_{neg} = 1.5E^* \sqrt{(I_{1\alpha}^-)^2 + (I_{1\beta}^-)^2} \quad (18)$$

$$Q_{ha5} = 1.5E^* \sqrt{(I_{5\alpha}^-)^2 + (I_{5\beta}^-)^2} \quad (19)$$

$$Q_{ha7} = 1.5E^* \sqrt{(I_{7\alpha}^+)^2 + (I_{7\beta}^+)^2} \quad (20)$$

where $I_{1\alpha}^+$ and $I_{1\beta}^+$ are the fundamental positive sequence current components; $I_{1\alpha}^-$ and $I_{1\beta}^-$ are the fundamental negative sequence current components; $I_{5\alpha}^-$ and $I_{5\beta}^-$ are the fifth harmonic current components; and $I_{7\alpha}^+$ and $I_{7\beta}^+$ are the seventh harmonic current components. As high order harmonic currents are relatively small, they are ignored in the proposed strategy.

3.1.2. Virtual Impedance Control

In this paper, the imbalance and harmonic powers are both regulated through virtual impedances. Referring to the relationship between the power and line impedance, the virtual impedance controller can be designed as

$$R_{v_neg,i} = R_{v_neg,i}^* + k_{neg,i} \delta_{v_neg,i} \quad (21)$$

$$R_{v_ha5,i} = R_{v_ha5,i}^* + k_{ha5,i} \delta_{v_ha5,i} \quad (22)$$

$$R_{v_ha7,i} = R_{v_ha7,i}^* + k_{ha7,i} \delta_{v_ha7,i} \quad (23)$$

where $R_{v_neg,i}^*$ is the virtual resistance at the fundamental negative sequence in the DG unit i ; $R_{v_ha5,i}^*$ and $R_{v_ha7,i}^*$ are the virtual resistances at the fifth and seventh harmonic frequencies in the DG unit i ; $\delta_{v_neg,i}$, $\delta_{v_ha5,i}$ and $\delta_{v_ha7,i}$ are the corresponding virtual resistance correction terms; and $k_{neg,i}$, $k_{ha5,i}$ and $k_{ha7,i}$ are the corresponding proportional gains.

The distributed consensus protocol is designed to generate virtual impedance correction terms $\delta_{v_neg,i}$, $\delta_{v_ha5,i}$, and $\delta_{v_ha7,i}$ through PI controllers to drive the imbalance and harmonic powers to be well shared. In this paper, power sharing based on a distributed controller is realized by constructing multi-agent systems. The power sharing problem can be considered as a regulator synchronization problem; $niQ_{neg,i}$, $niQ_{ha5,i}$, and $niQ_{ha7,i}$ can be considered as the state variables from the perspective of control theory. And, the control inputs are as follows:

$$u_{neg,i} = n_i \dot{Q}_{neg,i} \quad (24)$$

$$u_{ha5,i} = n_i \dot{Q}_{ha5,i} \quad (25)$$

$$u_{ha7,i} = n_i \dot{Q}_{ha7,i} \quad (26)$$

where $u_{neg,i}$, $u_{ha5,i}$, and $u_{ha7,i}$ are the auxiliary control inputs for the imbalance and fifth and seventh harmonic powers, respectively; $\dot{Q}_{neg,i}$, $\dot{Q}_{ha5,i}$, and $\dot{Q}_{ha7,i}$ are the variations of the

imbalance and fifth and seventh harmonic powers, respectively. To achieve the consensus of the system, the power information from the local DG unit and the neighbor DG units are utilized to construct the auxiliary control inputs:

$$\begin{aligned} u_{neg,i} &= -C_{neg}e_{neg,i} \\ &= -C_{neg} \sum_{j \in N_i} a_{ij} (n_i Q_{neg,i} - n_j Q_{neg,j}) \end{aligned} \quad (27)$$

$$\begin{aligned} u_{ha5,i} &= -C_{ha5}e_{ha5,i} \\ &= -C_{ha5} \sum_{j \in N_i} a_{ij} (n_i Q_{ha5,i} - n_j Q_{ha5,j}) \end{aligned} \quad (28)$$

$$\begin{aligned} u_{ha7,i} &= -C_{ha7}e_{ha7,i} \\ &= -C_{ha7} \sum_{j \in N_i} a_{ij} (n_i Q_{ha7,i} - n_j Q_{ha7,j}) \end{aligned} \quad (29)$$

where C_{neg} , C_{ha5} , and C_{ha7} are the coupling gains; $e_{neg,i}$ is the sum of the imbalance power sharing errors from the local DG unit i and its neighbor DG units; and $e_{ha5,i}$ and $e_{ha7,i}$ are the sum of the fifth and seventh harmonic power sharing errors, respectively. It can be proved that when the system steady state is achieved, $n_i Q_{neg,i} = n_j Q_{neg,j}$, $n_i Q_{ha5,i} = n_j Q_{ha5,j}$, and $n_i Q_{ha7,i} = n_j Q_{ha7,j}$. That means the reactive, imbalance, and harmonic power of the load will be properly shared by the DG units. The proposed adaptive virtual impedance regulation is sketched in Figure 4.

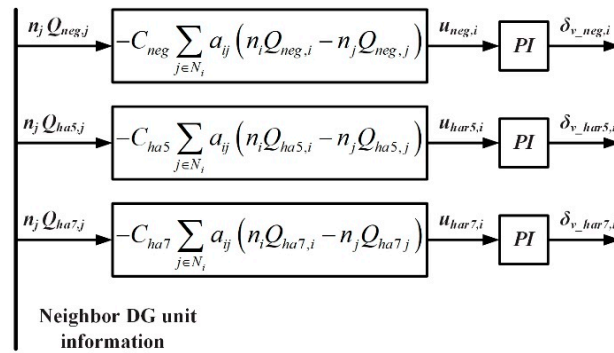


Figure 4. Proposed virtual resistance regulation in the DG unit.

Then, the virtual impedance correction terms $\delta_{v_neg,i}$, $\delta_{v_ha5,i}$, and $\delta_{v_ha7,i}$ are added to regulate $R_{v_neg,i}$, $R_{v_ha5,i}$, and R_{v_ha7} . In the proposed strategy, virtual reactance at each frequency is constant while the virtual resistance is variable as designed in (21)–(23).

3.2. P-F Regulator for Real Power Allocation and Frequency Restoration

The traditional frequency droop control method can realize accurate real power sharing; however, the economic factors are ignored. When communication is introduced, the economic operation of the system should be taken into account. Referring to the EIP in the traditional power system, the frequency droop control Equation (1) can be rewritten as:

$$\omega_i = \omega_{0i} - k\eta_i(P_i) \quad (30)$$

where $\eta_i(P_i)$ is the cost increment value (CIV) function, which is the derivative of the generation cost function $GC_i(P_i)$ with respect to P_i for DG unit i , and k is a positive scalar coefficient. In the steady state, the frequency of each DG unit must be equal [22]. Therefore, the $k\eta_i(P_i)$ of each DG unit is also equal, which meets the EIP of the economic dispatch (ED). The corresponding EIP regulator synchronization equation is as follow:

$$\begin{aligned} u_{p,i} &= -C_p e_{p,i} \\ &= -C_p \sum_{j \in N_i} a_{ij} [k\eta_i(P_i) - k\eta_j(P_j)] \end{aligned} \quad (31)$$

where C_p is the positive control gain for the EIP. On the other hand, to realize the restoration of the microgrid frequency, a tracking synchronization equation is added.

$$\begin{aligned} u_{\omega,i} &= -C_{\omega}e_{\omega,i} \\ &= -C_{\omega} \sum_{j \in N_i} \left[a_{ij}(\omega_i - \omega_j) + g_i(\omega_i - \omega_{ref}) \right] \end{aligned} \tag{32}$$

where C_{ω} is the positive control gain for the frequency tracking. When C_p and C_{ω} are equal, Equations (31) and (32) can be combined as

$$\begin{aligned} u_{\omega 0,i} &= u_{\omega p,i} + u_{\omega,i} = -C_{\omega}e_{\omega,i} - C_p e_{p,i} \\ &= -C_{\omega} \sum_{j \in N_i} \left[a_{ij}(\omega_{0i} - \omega_{0j}) + g_i(\omega_i - \omega_{ref}) \right] \end{aligned} \tag{33}$$

The corresponding frequency regulation is sketched in Figure 5.

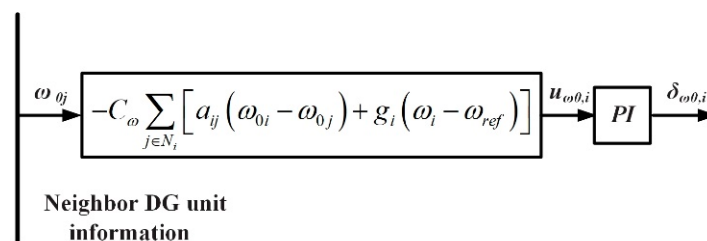


Figure 5. Proposed frequency regulation in the DG unit.

In the Figure 4, $\delta_{\omega 0,i}$ is the frequency correction term, which will be added to $\omega_{0,i}$ in (30) as:

$$\omega_i^* = \omega_{0i} - k\eta_i(P_i) + \delta_{\omega 0,i} \tag{34}$$

With the frequency regulator and tracking equations, the system is maintained at the rated frequency, and each DG unit keeps the equal cost increment. Compared with real power sharing principle, the system with the EIP has a much lower generation cost.

3.3. Q-V Regulator for Reactive Power Sharing and Voltage Restoration

The reason for inaccurate reactive power sharing is the different voltage drops of the line impedances of the DG units. Thus, a voltage correction term $\delta_{q,i}$ is added to (2), which is generated through a PI controller. The corresponding controller input is as follow:

$$\begin{aligned} u_{q,i} &= -C_q e_{q,i} \\ &= -C_q \sum_{j \in N_i} a_{ij} (n_i Q_i - n_j Q_j) \end{aligned} \tag{35}$$

where C_q is the coupling gain and $e_{q,i}$ is the sum of the reactive power sharing errors from the local DG unit i and its neighbor DG units. With this regulator synchronization equation, at steady state, $n_i Q_i = n_j Q_j$. On the other hand, to better realize the seamless switching of the microgrid, the proposed control strategy will keep the PCC voltage at the rated value. So the tracking synchronization equation is added.

$$\begin{aligned} u_{pcc,i} &= -C_{pcc} e_{pcc,i} \\ &= -C_{pcc} \sum_{j \in N_i} \left[a_{ij} (E_{0i} - E_{0j}) + g_i (E_i - E_{ref}) \right] \end{aligned} \tag{36}$$

where C_{pcc} is a positive control gain and E_{ref} is selected through a PI controller, so that the PCC voltage E_{pcc} can recover to its reference rated value E_{pcc}^* with zero error. The proposed PCC voltage and reactive power regulation is sketched in Figure 6.

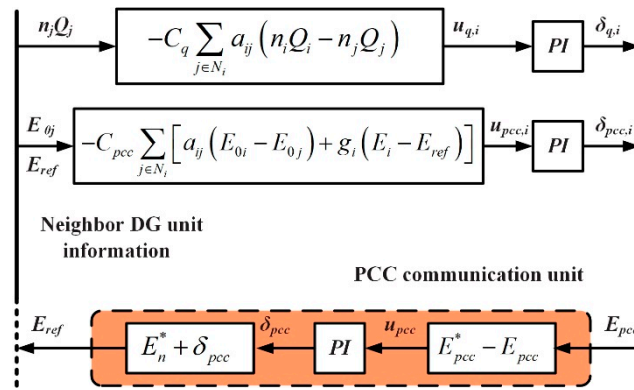


Figure 6. Proposed voltage regulation in the DG unit.

In the figure, $\delta_{pcc,i}$ and $\delta_{q,i}$ are the voltage correction terms, which are added to E_i^* in (2) as:

$$E_i = E_{0i} - n_i Q_i + \delta_{q,i} + \delta_{pcc,i} \tag{37}$$

The value of E_{ref} is calculated in the PCC monitor unit, which is treated as a communication node in the microgrid and also participates in voltage regulation. The E_{ref} is selected through a PI controller such that E_{PCC} recovers to its reference rated value E_{PCC}^* with zero error. Its calculation process is as follows:

$$E_{ref} = E_n^* + k_p \Delta E_{pcc} + k_I \int \Delta E_{pcc} dt \tag{38}$$

$$\Delta E_{pcc} = E_{pcc}^* - E_{pcc} \tag{39}$$

where k_p and k_I are the gains of the PI controller in the PCC monitor. When the voltage regulation (35)~(37) converges to the steady state, $u_{pcc,i}$ and the output of the PI controller in (38) converge to steady-state values; then, the E_i of each DG unit converges to have the same $n_i Q_i$, and the PCC voltage reaches the reference value E_{PCC}^* .

3.4. Overall Control Diagram

Figure 7 illustrates a schematic of the proposed control strategy. The DG unit controller consists of several separate modules. Some are basic modules: the droop controller and proportional resonance (PR) controller; some are consensus-based modules: the I-H regulator, P-F regulator, and Q-V regulator; and the others are auxiliary modules: the power calculation module, the virtual impedance module, and the virtual voltage calculation module.

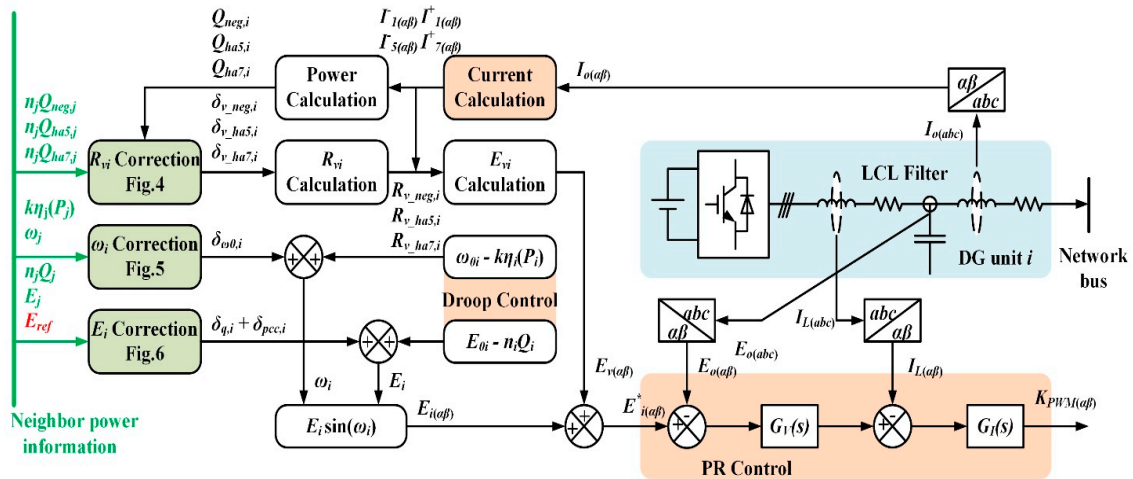


Figure 7. Control diagram of the proposed strategy.

The virtual voltage E_{vi} calculation after virtual impedance regulation is as follows:

$$E_{v_{\alpha,i}} = \left(R_{v_{neg,i}} I_{1\alpha,i}^- + X_{v_{neg,i}} I_{1\beta,i}^- \right) + \left(R_{v_{ha5,i}} I_{5\alpha,i}^- + X_{v_{ha5,i}} I_{5\beta,i}^- \right) + \left(R_{v_{ha7,i}} I_{7\alpha,i}^+ - X_{v_{ha7,i}} I_{7\beta,i}^+ \right) \tag{40}$$

$$E_{v_{\beta,i}} = \left(R_{v_{neg,i}} I_{1\beta,i}^- - X_{v_{neg,i}} I_{1\alpha,i}^- \right) + \left(R_{v_{ha5,i}} I_{5\beta,i}^- - X_{v_{ha5,i}} I_{5\alpha,i}^- \right) + \left(R_{v_{ha7,i}} I_{7\beta,i}^+ + X_{v_{ha7,i}} I_{7\alpha,i}^+ \right) \tag{41}$$

To ensure voltage tracking, a double-loop voltage control with harmonic voltage compensators is adopted. The outer loop is an LCL filter capacitor voltage control loop $G_V(s)$ and the inner loop is an inverter output current control loop $G_I(s)$ as follows:

$$G_V(s) = k_{pV} + \sum_{h=1,5,7,\dots} \frac{2k_{vh}\omega_b s}{s^2 + 2\omega_b s + (h\omega^*)^2} \tag{42}$$

$$G_I(s) = k_{pI} \tag{43}$$

where k_{vh} is the gain of the resonant controllers in the outer voltage control loop; ω_b is the bandwidth of the resonant controllers; and k_{pV} and k_{pI} are the proportional gains of the voltage and current controllers, respectively.

The I-H regulator is developed to enable the DG units to proportionally share the imbalance and harmonic loads. The Q-V regulator can enhance the accuracy of reactive power sharing and the voltage quality at the PCC. The P-F regulator can ensure the equal increment operation of DG units and maintain the microgrid frequency rated values. The controller at DG unit i receives information from its neighbors ($n_j Q_{neg,j}$, $n_j Q_{ha5,j}$, $n_j Q_{ha7,j}$, $k_{\eta j}(P_j)$, ω_j , $n_j Q_j$, E_j , and E_{ref}), and processes the neighbor units' and local data ($n_i Q_{neg,i}$, $n_i Q_{ha5,i}$, $n_i Q_{ha7,i}$, $k_{\eta i}(P_i)$, ω_i , $n_i Q_i$, and E_i) to generate the correction terms ($\delta_{v_{neg,i}}$, $\delta_{v_{ha5,i}}$, $\delta_{v_{ha7,i}}$, $\delta_{p,i}$, $\delta_{\omega,i}$, $\delta_{q,i}$, and $\delta_{pcc,i}$) of the virtual impedance, frequency, and voltage through corresponding PI controllers. It can be seen that the controller at each inverter is totally distributed and that each controller only uses the information of its local and neighbor units, which can be more flexible and reliable.

4. Simulation Results

To test the performance of the proposed control strategy, a microgrid with four DG units was simulated in MATLAB/Simulink environment. The structure of the test microgrid is illustrated in Figure 8.

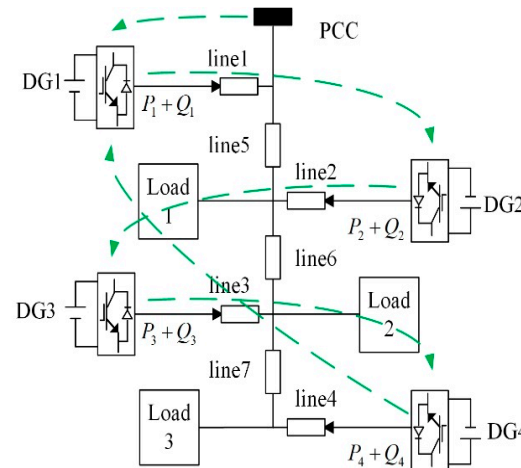


Figure 8. A schematic diagram of the test microgrid.

Table 1 provides the system and the DG primary control parameters. The reactive power capacities of the DG units are set to be the same. Thus, in an ideal situation, the reactive power of the DG units should be equal. The cost parameters for the DG units are given in Table 2. By taking the derivative of P, the cost increment function can be obtained.

Table 1. Electrical parameters of the microgrid.

Circuit Parameters		Values
Line 1–7	Resistance	$R_f = [1\ 1\ 4\ 3\ 1\ 1\ 1] * 0.1\ \Omega$
	Resistance	$X_f = [1\ 1\ 4\ 3\ 1\ 1\ 1] * 0.028j\ \Omega$
DG 1–4	LC Filter	$L_f = 1.5\ \text{mH}, C_f = 100\ \mu\text{F}$
	Frequency	$f_s = 10\ \text{kHz}$
	Capacity	$S = 25\ \text{kVA}$
Load 1–3	Real power	$P_L = 25\ \text{kW}$
	Reactive power	$Q_L = 20\ \text{kVar}$
Droop	Droop Slopes	$D_p = 8 \times 10^{-6}, D_q = 1 \times 10^{-4}$
	Initial Voltage	$E_0 = 320\ \text{V}, F_0 = 50.125\ \text{Hz}$
PR	Voltage Controller	$k_p = 0.1, k_{1h} = 20, k_{5h} = k_{7h} = 15$
	Current Controller	$k_p = 0.1$
Consensus	Q regulator	$k_p = 4 \times 10^{-4}, k_p = 1.6 \times 10^{-3}$
	V regulator	$k_p = 0, k_I = 0.5$
	P-f regulator	$k_p = 0, k_I = 8 \times 10^{-4}$
	I-H regulator	$k_p = 0, k_I = 2.5 \times 10^{-5}$
Load Condition		Remarks
Test 1	Three-phase balanced Load	Remove Load2 at $t = 4\ \text{s}$
Test 2	Imbalanced Load Diode Rectifier	Remove phase C loads in Test 1 $R_d = 8\ \Omega, C_d = 5\ \mu\text{F}$

Table 2. Cost Parameters of the DG units.

	Cost Function
DG 1	$0.094P^2 + 1.22P + 51$
DG 2	$0.078P^2 + 3.41P + 31$
DG 3	$0.105P^2 + 2.53P + 78$
DG 4	$0.082P^2 + 4.02P + 42$

The SCN of the microgrid is also shown in Figure 8. In the test system, DG 1 receives information from DG 4, DG 2 receives information from DG 1, DG 3 receives information from DG 2, and DG 4 receives information from DG 3. Figure 8 also indicates that DG 1–4 are all root nodes, and DG 1 is the only root node with the reference value and the pinning gain of $g_1 = 1$.

4.1. Economic Operation Test

In this simulation test, the microgrid connects three-phase balanced loads and operate with the traditional droop control method and the proposed method, respectively.

(1) Case 1: Traditional droop control method:

The performance of the system with the traditional droop control method is shown in Figure 9. Figure 9a,b show the real and reactive powers of DG units in Case 1, respectively. At $t = 4\ \text{s}$, Load 2 is removed from the network. As can be seen from the figure, the output powers of DG 1–4 decrease at the same time. As analyzed before, due to the same frequency among the DG units, the load real power is well shared. In an ideal situation, the DG output reactive power should be proportional to the DG capacity: that is, Q_1, Q_2, Q_3 , and

Q_4 should be equal in the simulation. However, due to the mismatched feeder lines, the load reactive power has many sharing errors.

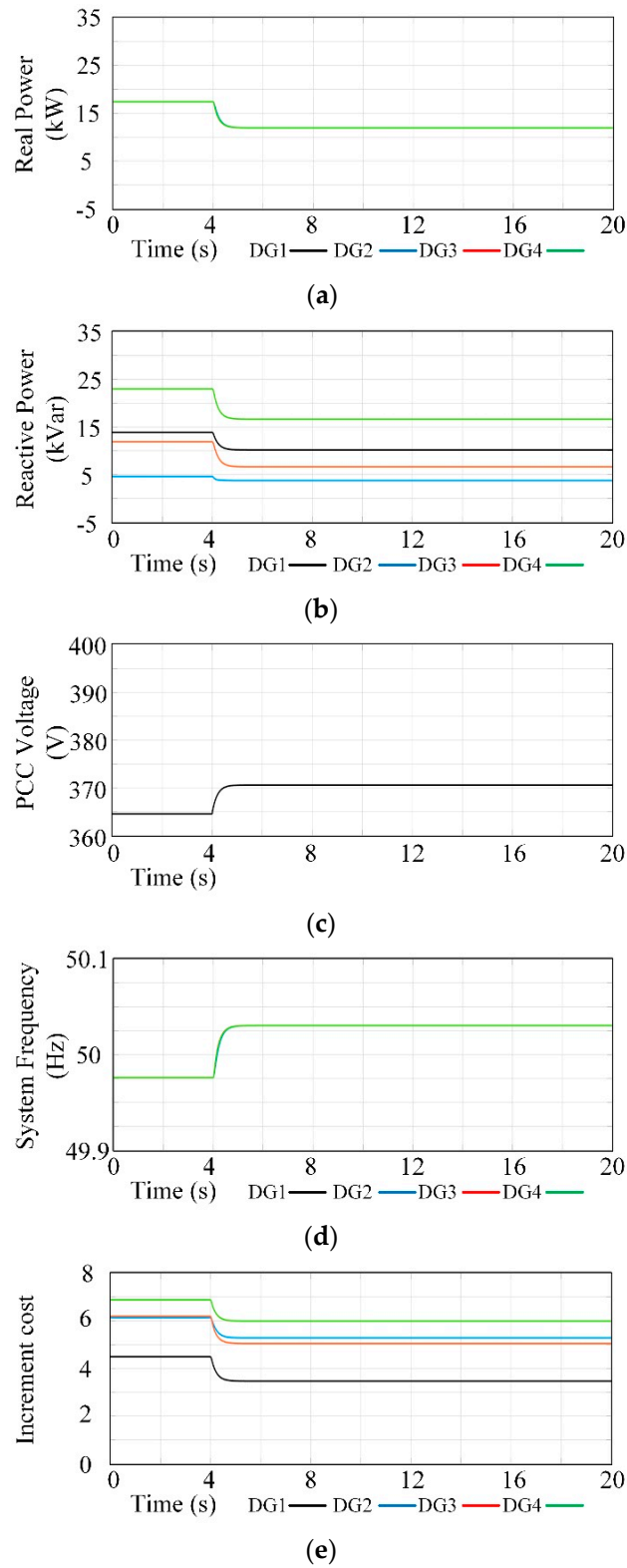


Figure 9. System performance of the microgrid in Case 1. (a) Real power of DG units. (b) Reactive power of DG units. (c) Voltage magnitude of the PCC. (d) System frequency. (e) Incremental cost of DG units.

Figure 9c shows the magnitude of the voltage at the PCC. And Figure 9d shows the frequency of the test microgrid. According to the deviating regulation characteristics of droop control, the system frequency is not 50 Hz; meanwhile, the PCC voltage is not 380 V. The voltage is determined by the reactive load in the system.

Figure 9e shows the incremental cost of each DG unit of the system using the droop control. At this point, these DG incremental costs are different. The total power generation cost before and after load change is 509 and 389, respectively. The results will be compared with the cost of the system using the proposed strategy in the next section.

(2) Case 2: Consensus-based control strategy:

In Case 2, DG 1–4 adopt the proposed control strategy. As in Case 1, Load 2 is removed from the network at $t = 4$ s. Figure 10 shows the corresponding system performance. Figure 10a,b show the real and reactive power of DG units in Case 2, respectively. As the figure shows, the output real power of DG 1–4 is no longer equal, but according to the EIP, this can make the total power generation cost of the system the lowest. It can be seen from Figure 10b that the output reactive power of DG 1–4 is equal, which means the accurate reactive power sharing has been realized.

Figure 9c,d show the frequency and voltage of the test microgrid. As the figure shows, due to the tracking control of the consensus algorithm, the system frequency and the PCC voltage are always at the rated values.

Figure 9e shows the incremental cost of each DG unit, the total power generation cost before and after load change is 344 and 246, respectively. As the increment costs of DG units are all the same, and the total generation cost has been significantly reduced compared with that in Case 1. Thus, the economic operation has been realized.

4.2. Current Sharing Test

In this simulation test, the current sharing performance of the proposed strategy is verified. Since the reactive power sharing function has been tested above, only the imbalanced and harmonic power sharing functions are tested next.

(1) Case 3: Imbalanced Power Sharing:

In this test, the DG units adopt the proposed control strategy, and for ease of comparison, the DG units are set to have the same cost function. At the beginning, the I-H regulator is disabled. The performance of the strategy in imbalanced load condition is shown in Figure 11. Figure 11a,b show the fundamental real and reactive power of the DG units. Due to the work of the P-f and Q-V regulators, the real powers of DG units are always equal, as well as the reactive power. But the DG output imbalanced powers are quite different initially, as shown in Figure 11c.

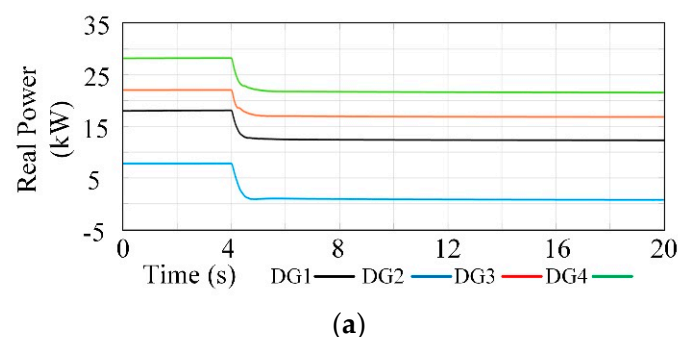


Figure 10. Cont.

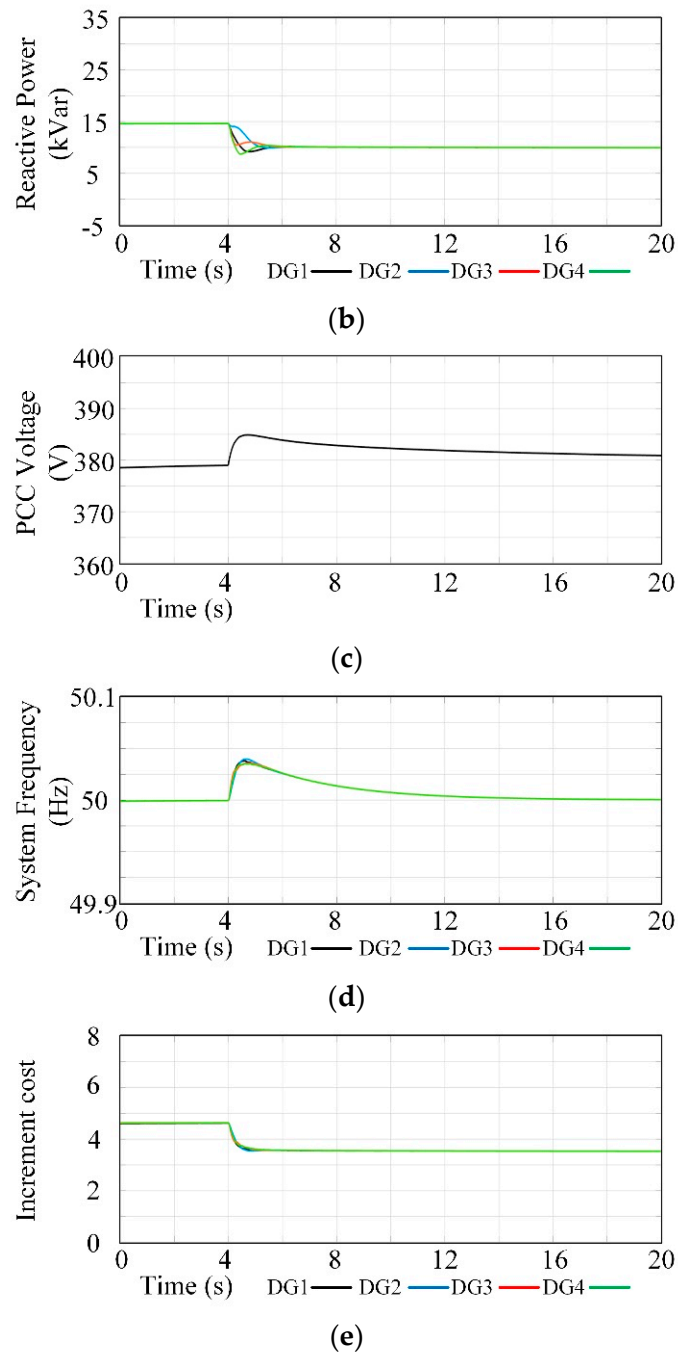


Figure 10. System performance of the microgrid in Case 2. (a) Real power of DG units. (b) Reactive power of DG units. (c) Voltage magnitude of the PCC. (d) System frequency. (e) Incremental cost of DG units.

The I-H regulator is enabled at $t = 4$ s. As can be seen from Figure 11c, the imbalance powers begin to converge. The change in imbalance powers directly reflects the change in currents. The DG currents before and after the I-H regulator works are shown in Figure 11d. Due to the phase loss, the three-phase currents of the DG units are imbalanced. In an ideal situation, the corresponding phase current of each DG unit should be equal, and the currents in phase C should be 0. However, there are significant circulation currents in the system, which is far from the ideal case. After the I-H regulator works, the phase C currents are reduced to zero, and the DG currents in each phase are equal. The circulation current is eliminated.

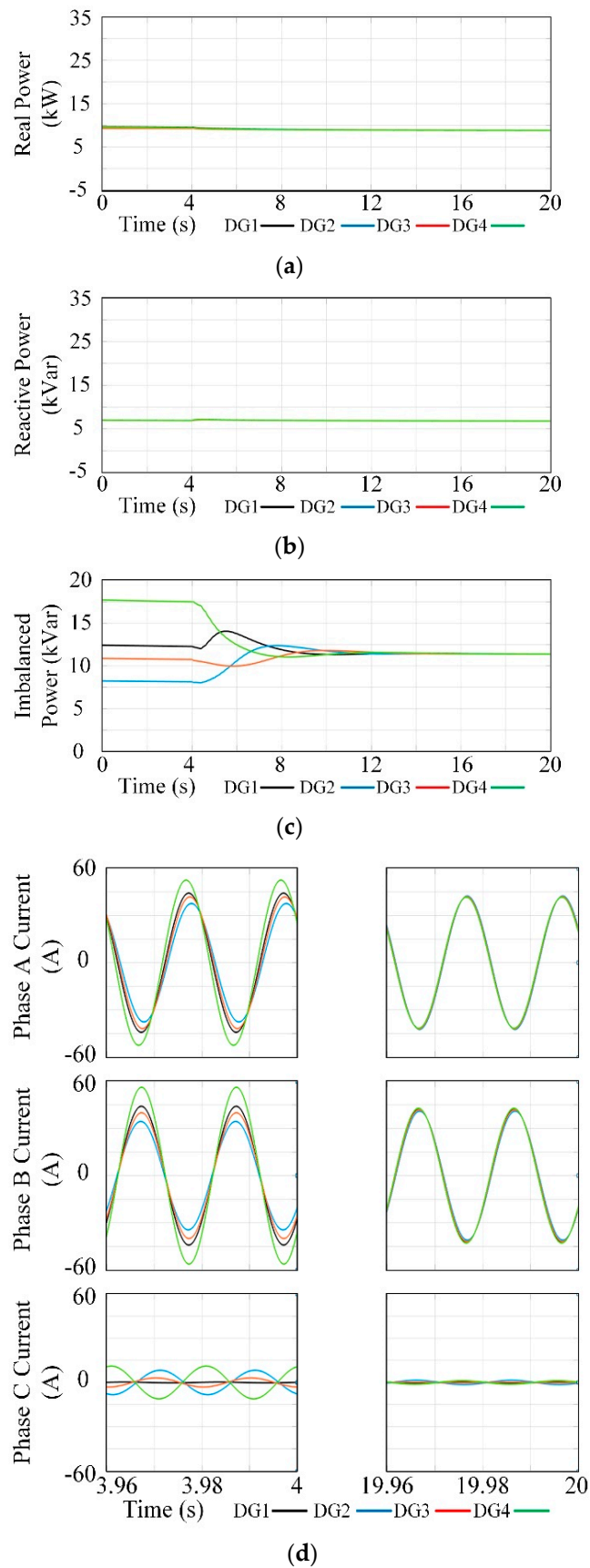


Figure 11. System performance of the microgrid in Case 3. (a) Real power of DG units. (b) Reactive power of DG units. (c) Imbalance power of DG units. (d) Currents before and after I-H regulator enabled.

(2) Case 4: Harmonic power sharing

In this simulation case, the loads in Case 3 are replaced by three-phase rectifier bridges. Similarly, the I-H regulator is enabled at $t = 4$ s. Figure 12a,b show the fundamental real and reactive power of the DG units. All the DG units can output the same real and reactive powers when adopting the proposed strategy. Otherwise, the reactive power sharing error will make the current sharing performance even poorer. Since the I-H regulator is disabled at the beginning, the load fifth and seventh harmonic powers have not been well shared, as shown in Figure 11c,d, respectively.

After $t = 4$ s, the I-H regulator begins to work. The DG output fifth and seventh powers begin to converge, respectively. The corresponding DG currents before and after the I-H regulator works are shown in Figure 12e. Before $t = 4$ s, the harmonic currents are different in phases and magnitudes, leading to the poor performance of system current sharing. However, they are almost the same after the regulation of virtual impedance being completed, as Figure 12e shows.

Through the two simulation tests, the economic operation and current sharing functions of the proposed strategy have both been verified.

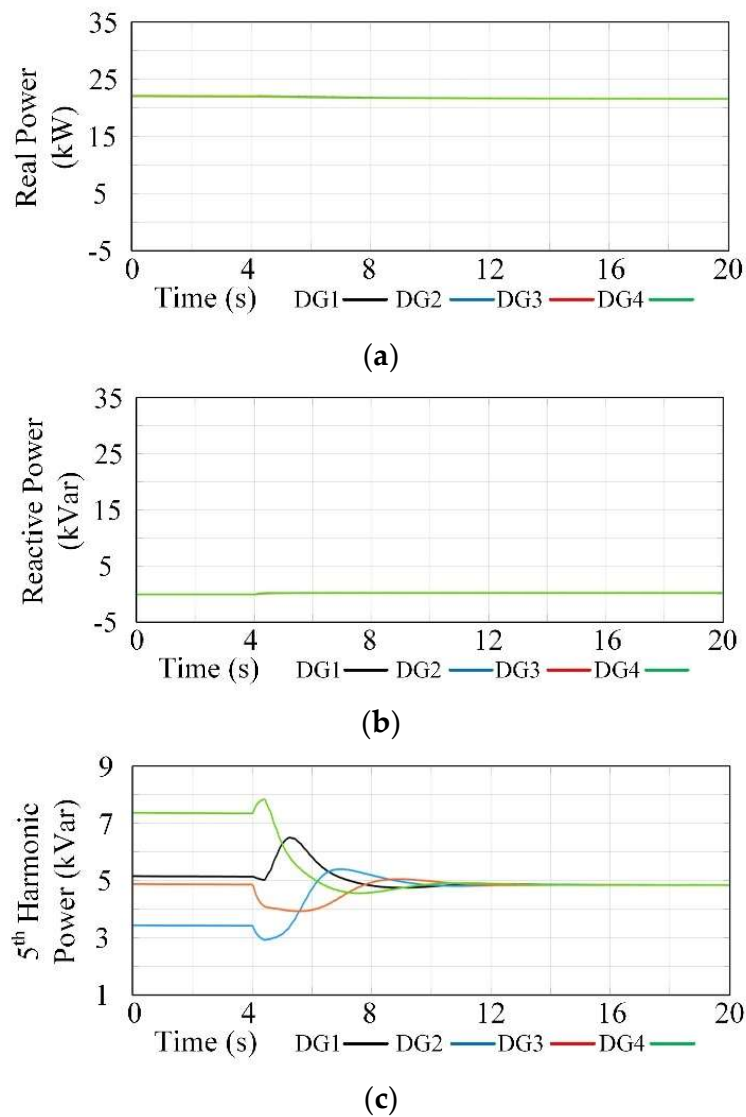


Figure 12. Cont.

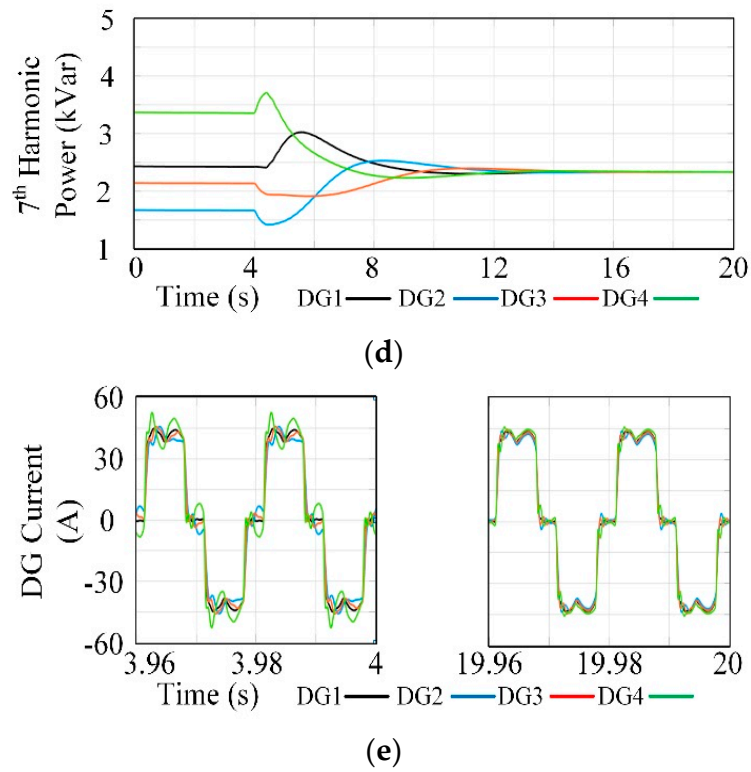


Figure 12. System performance of the microgrid in Case 4. (a) Real power of DG units. (b) Reactive power of DG units. (c) Fifth harmonic power of DG units. (d) Seventh harmonic power of DG units. (e) Currents before and after I-H regulator enabled.

5. Experimental Results

Experiments are performed to validate the effectiveness of the proposed consensus-based control strategy. A microgrid with three inverters is established in a laboratory, as shown in Figure 13. This experiment is mainly to verify the reactive, imbalance, and harmonic power sharing functions of the strategy. The corresponding inverter parameters are listed in Table 3.

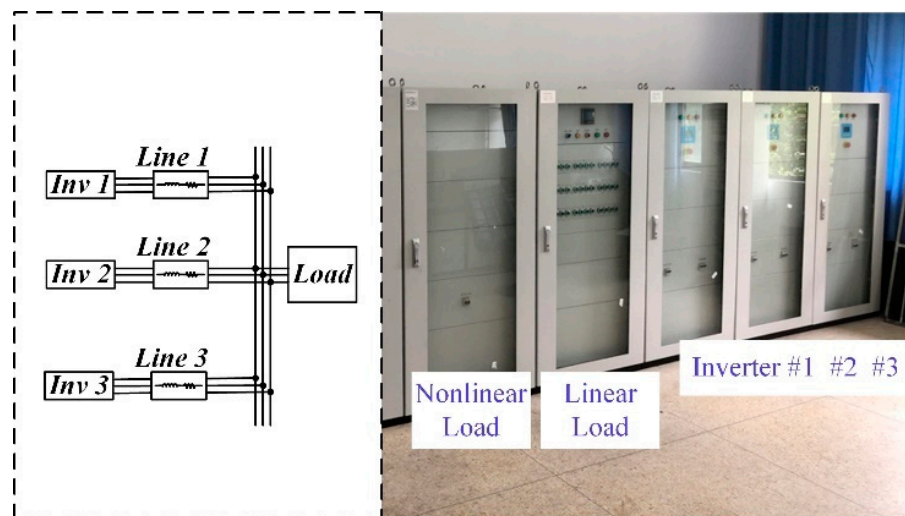


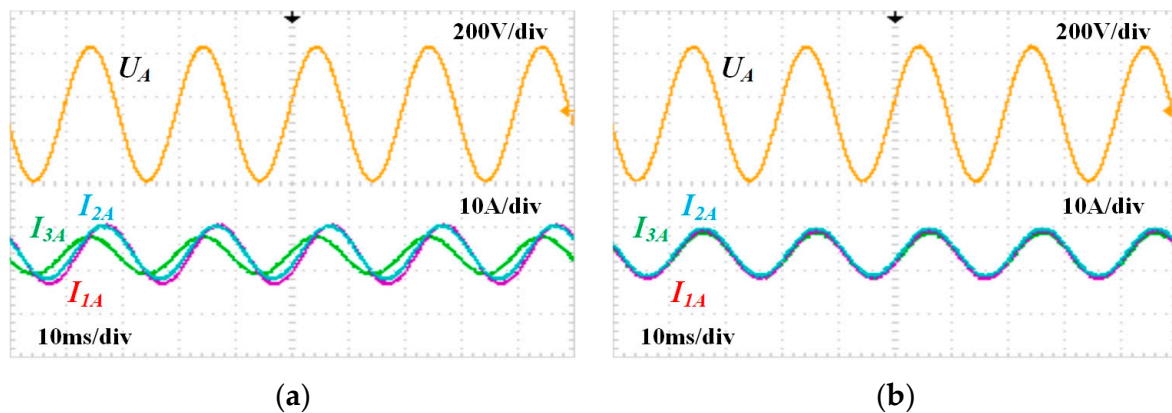
Figure 13. Structure of the experimental microgrid.

Table 3. The corresponding inverter parameters.

Circuit Parameters		Values
Feeder Line	Feeder 1	$R_{f1} = 0.10 \Omega$
	Feeder 2	$R_{f2} = 0.05 \Omega$
	Feeder 3	$R_{f3} = 0.15 \Omega$
Inverter	LC Filter	$L_f = 0.7 \text{ mH}, C_f = 50 \mu\text{F}$
	Frequency	$f_s = 10 \text{ kHz}$
Control Parameters		Values
Inv 1–3	Droop Slopes	$m = 5 \times 10^{-6}, n = 5 \times 10^{-5}$
	Initial Voltage	$E_0 = 315 \text{ V}, F_0 = 50.15 \text{ Hz}$
	Voltage Controller	$k_{pV} = 7.6, k_{IV} = 76$
	Current Controller	$k_{pI} = 0.2, k_{II} = 15$

(1) Case 1: Reactive Power Sharing:

In this experimental case, a three-phase linear balanced load is connected to the test system. The currents in phase A of the inverters using the traditional droop control method are shown in Figure 14a. Due to the different feeder impedances, the inverters output different currents at the beginning. As Feeder 3 has the highest resistance, the voltage of inverter 3 is higher than the other two. According to the Q-V droop control relationship, inverter 3 outputs the least reactive power. Thus, I_{3A} advances I_{1A} and I_{2A} , and has the min magnitude. After the proposed strategy operates, the currents of the three inverters are equal, as shown in Figure 14b, proving that the real and reactive powers have been well shared.

**Figure 14.** Currents of the inverters. (a) With the traditional method in experimental Case 1. (b) With the proposed method in experimental Case 1.

(2) Case 2: Imbalanced Power Sharing:

By floating phase C of the load in Case 1, an unbalanced load is obtained. Figure 15a illustrates the currents of the three inverters using the traditional droop control method. As the load is unbalanced, there are significant negative sequence currents in the system. After the proposed strategy starts, the output currents of inverters become equal, as shown in Figure 15b, and current in phase C is almost zero. The negative sequence current is eliminated.

(3) Case 3: Harmonic Power Sharing:

Finally, the proposed consensus-based control strategy is tested in a nonlinear load condition. The performance of the system with the traditional droop control method is shown in Figure 16a. As the load harmonic power has not been well shared, the currents of the inverters are quite different. Then, the proposed strategy is enabled in each inverter,

making their output current almost the same, as shown in Figure 16b. The harmonic power output of the inverter tends to be the same.

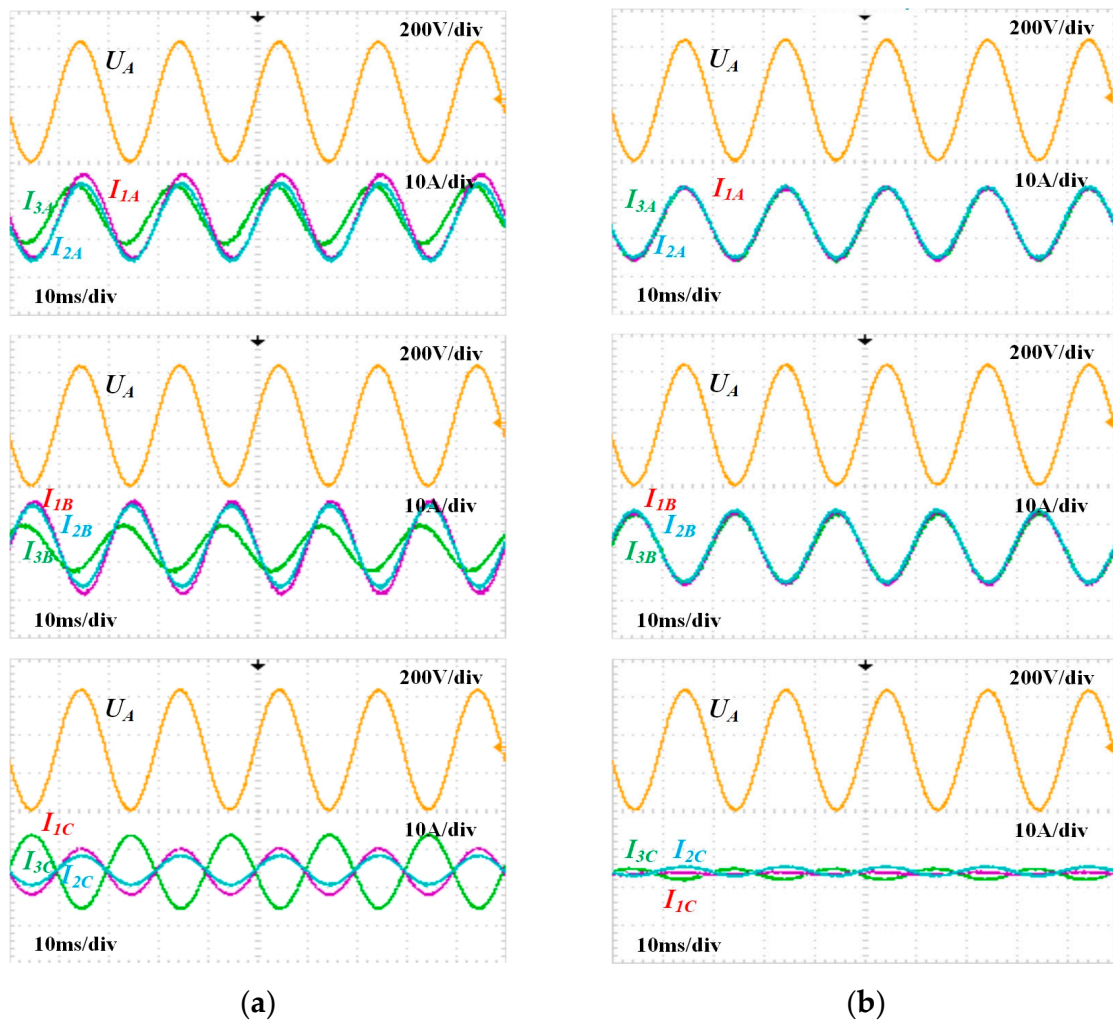


Figure 15. Currents of the inverters. (a) With the traditional method in experimental Case 2. (b) With the proposed method in experimental Case 2.

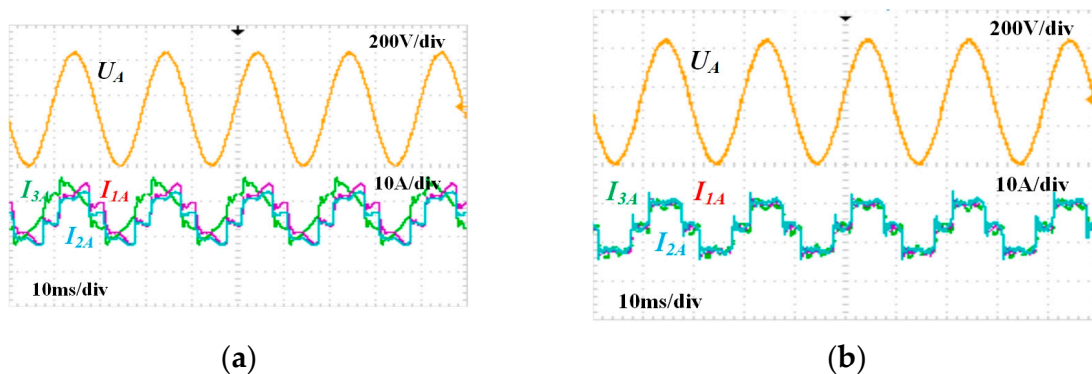


Figure 16. Currents of the inverters. (a) With the traditional method in experimental Case 3. (b) With the proposed method in experimental Case 3.

6. Conclusions

In this paper, a consensus-based control strategy is proposed for the microgrid to simulate power allocation issues, in which the fundamental real power is allocated according

to the equal micro-increment rate, and the fundamental reactive power, imbalance, and harmonic power are allocated according to the DG capacity. And, in the harmonic power sharing process, a frequency division power control method based on virtual resistance is proposed. The proposed frequency division control can share the harmonic power of each frequency more effectively compared with traditional harmonic sharing control. From results obtained by Matlab simulations and experiments, it can be seen that the preset targets are all achieved. With the proposed strategy, the performance of the droop control method is improved, and compared with the MGCC-based secondary control strategy, the SCN-based distributed control strategy has little effect on the “plug and play” functions.

Author Contributions: Conceptualization, data curation, formal analysis, investigation, methodology, writing—original draft, and writing—review and editing, C.Y.; conceptualization, methodology, writing—original draft, and writing—review and editing, X.W.; methodology, writing—original draft, and writing—review and editing, Q.S.; writing—original draft and writing—review and editing, H.W. and Y.Z. All authors have read and agreed to the published version of the manuscript.

Funding: This research was funded by the 74th batch of general support from the China Postdoctoral Foundation (Grant No. 2023M742386).

Data Availability Statement: No new data were created or analyzed in this study. Data sharing is not applicable to this article.

Conflicts of Interest: The authors declare that the research was conducted in the absence of any commercial or financial relationships that could be construed as a potential conflict of interest.

Abbreviations

The following abbreviations are used in this manuscript:

DG	Distributed Generation
SOGI	Second-order Generalized Integrator
PCC	Point Of Common Coupling
MGCC	Management Of Microgrid Central Controller
SCN	Sparse Communication Network
EIP	Equal Increment Principle
STS	Static Transfer Switch
PNSC	Positive/Negative Sequence Calculation
PR	Proportional Resonance

References

1. Yin, M.; Li, K.; Yu, J. A data-driven approach for microgrid distributed generation planning under uncertainties. *Appl. Energy* **2022**, *309*, 118429. [[CrossRef](#)]
2. Xu, H.; Zhang, X.; Liu, F.; Shi, R.; Yu, C.; Cao, R. A reactive power sharing strategy of VSG based on virtual capacitor algorithm. *IEEE Trans. Ind. Electron.* **2017**, *64*, 7520–7531. [[CrossRef](#)]
3. Xiong, L.; Liu, X.; Liu, Y.; Zhuo, F. Modeling and stability issues of voltage-source converter dominated power systems: A review. *CSEE J. Power Energy Syst.* **2022**, *8*, 1530–1549.
4. Liu, X.; Du, Z.; Tan, Y.; Liu, Y. Voltage Optimization Control Strategy for Islanded Microgrid Source-Grid-Load Active-Reactive Power Coordination Based on Collaborative Di-MPC. *Front. Energy Res.* **2022**, *10*, 880825. [[CrossRef](#)]
5. Wong, Y.C.C.; Lim, C.S.; Rotaru, M.D.; Cruden, A.; Kong, X. Consensus Virtual Output Impedance Control Based on the Novel Droop Equivalent Impedance Concept for a Multi-Bus Radial Microgrid. *IEEE Trans. Energy Convers.* **2020**, *35*, 1078–1087. [[CrossRef](#)]
6. Deng, F.; Yao, W.; Zhang, X.; Tang, Y.; Mattavelli, P. Review of Impedance-Reshaping-Based Power Sharing Strategies in Islanded AC Microgrids. *IEEE Trans. Smart Grid.* **2023**, *14*, 1692–1707. [[CrossRef](#)]
7. Deng, F.; Li, Y.; Li, X.; Yao, W.; Zhang, X.; Mattavelli, P. A Decentralized Impedance Reshaping Strategy for Balanced, Unbalanced and Harmonic Power Sharing in Islanded Resistive Microgrids. *IEEE Trans. Sustain. Energy* **2022**, *13*, 743–754. [[CrossRef](#)]
8. Zhu, Y.X.; Zhuo, F.; Wan, F.; Liu, B.Q.; Zhao, Y.J. A wireless load sharing strategy for islanded microgrid based on feeder current sensing. *IEEE Trans. Power Electron.* **2015**, *30*, 6706–6719. [[CrossRef](#)]
9. He, J.W.; Li, Y.W. An enhanced microgrid load demand sharing strategy. *IEEE Trans. Power Electron.* **2012**, *27*, 3984–3995. [[CrossRef](#)]

10. Han, H.; Liu, Y.; Sun, Y.; Su, M.; Guerrero, J.M. An improved droop control strategy for reactive power sharing in islanded microgrid. *IEEE Trans. Power Electron.* **2015**, *30*, 3133–3141. [[CrossRef](#)]
11. Liu, S.; Wang, X.; Liu, P.X. Impact of communication delays on secondary frequency control in an islanded microgrid. *IEEE Trans. Ind. Electron.* **2015**, *62*, 2021–2031. [[CrossRef](#)]
12. Hoang, T.V.; Lee, H. Accurate power sharing with harmonic power for islanded multi-bus microgrids. *IEEE J. Emerg. Sel. Top. Power Electron.* **2019**, *7*, 1286–1299. [[CrossRef](#)]
13. Li, S.; Wu, J.; Agundis-Tinajero, G.D.; Chaudhary, S.; Vasquez, J.C.; Guerrero, J.M. A Hierarchical Harmonic Control Method for Wind Power Plants in Microgrids. In Proceedings of the IECON 2023-49th Annual Conference of the IEEE Industrial Electronics Society, Singapore, 16–19 October 2023; pp. 1–6.
14. Chen, L.; Wang, Y.; Lu, X.; Zheng, T.; Wang, J.; Mei, S. Resilient active power sharing in autonomous microgrids using pinning-consensus-based distributed control. *IEEE Trans. Smart Grid.* **2019**, *10*, 6802–6811. [[CrossRef](#)]
15. Wang, Z.; Wu, W.; Zhang, B. A fully distributed power dispatch method for fast frequency recovery and minimal generation cost in autonomous microgrids. *IEEE Trans. Smart Grid.* **2016**, *7*, 19–31. [[CrossRef](#)]
16. Xiong, L.; Liu, L.; Liu, X.; Liu, Y. Frequency trajectory planning based strategy for improving frequency stability of droop-controlled inverter based standalone power systems. *IEEE J. Emerg. Sel. Top. Circuits Syst.* **2021**, *11*, 176–187. [[CrossRef](#)]
17. Schiffer, J.; Seel, T.; Raisch, J.; Sezi, T. Voltage stability and reactive power sharing in inverter-based microgrids with consensus based distributed voltage control. *IEEE Trans. Control Syst. Technol.* **2016**, *24*, 96–109. [[CrossRef](#)]
18. Lai, J.; Lu, X.; Li, X.; Tang, R. Distributed multiagent-oriented average control for voltage restoration and reactive power sharing of autonomous microgrids. *IEEE Access* **2018**, *6*, 25551–25561. [[CrossRef](#)]
19. Lu, J.; Zhao, M.; Golestan, S.; Dragicevic, T.; Pan, X.; Guerrero, J.M. Distributed Event-Triggered Control for Reactive, Unbalanced, and Harmonic Power Sharing in Islanded AC Microgrids. *IEEE Trans. Ind. Electron.* **2022**, *69*, 1548–1560. [[CrossRef](#)]
20. He, J.; Li, Y.W.; Blaabjerg, F. An enhanced islanding microgrid reactive power, imbalance power, and harmonic power sharing scheme. *IEEE Trans. Power Electron.* **2015**, *30*, 3389–3401. [[CrossRef](#)]
21. Meng, L.; Zhao, X.; Tang, F.; Dragicevic, T.; Savaghebi, M.; Vasquez, J.C.; Guerrero, J.M. Distributed voltage unbalance compensation in islanded microgrids by using dynamic consensus algorithm. *IEEE Trans. Power Electron.* **2016**, *31*, 827–838. [[CrossRef](#)]
22. Guo, F.; Wen, C.; Mao, J.; Chen, J.; Song, Y.D. Distributed cooperative secondary control for voltage unbalance compensation in an islanded microgrid. *IEEE Trans. Ind. Inform.* **2015**, *11*, 1078–1088. [[CrossRef](#)]
23. Zhou, J.; Kim, S.; Zhang, H.; Sun, Q.; Han, R. Consensus-based distributed control for accurate reactive, harmonic, and imbalance power sharing in microgrids. *IEEE Trans. Smart Grid.* **2018**, *9*, 2453–2467. [[CrossRef](#)]
24. Tang, Z.; Hill, D.J.; Liu, T. A novel consensus-based economic dispatch for microgrids. *IEEE Trans. Smart Grid* **2018**, *9*, 3920–3922. [[CrossRef](#)]
25. Zheng, Y.; Song, Y.; Hill, D.J.; Zhan, Y. Multiagent system based microgrid energy management via asynchronous consensus ADMM. *IEEE Trans. Energy Conv.* **2018**, *33*, 886–888. [[CrossRef](#)]
26. Wang, R.; Li, Q.; Zhang, B.; Wang, L. Distributed consensus-based algorithm for economic dispatch in a microgrid. *IEEE Trans. Smart Grid.* **2019**, *10*, 3630–3640. [[CrossRef](#)]
27. Wu, X.; Shen, C.; Iravani, R. A distributed, cooperative frequency and voltage control for microgrids. *IEEE Trans. Smart Grid.* **2018**, *9*, 2764–2776. [[CrossRef](#)]
28. Olfati-Saber, R.; Murray, R.M. Consensus problems in networks of agents with switching topology and time-delays. *IEEE Trans. Auto. Control* **2004**, *49*, 1520–1533. [[CrossRef](#)]
29. Li, Z.; Duan, Z.; Chen, G.; Huang, L. Consensus of Multiagent systems and synchronization of complex networks: A unified viewpoint. *IEEE Trans. Circuits Syst. I Regul. Pap.* **2010**, *57*, 213–224.

Disclaimer/Publisher’s Note: The statements, opinions and data contained in all publications are solely those of the individual author(s) and contributor(s) and not of MDPI and/or the editor(s). MDPI and/or the editor(s) disclaim responsibility for any injury to people or property resulting from any ideas, methods, instructions or products referred to in the content.